Alternative to the topological interpretation of the transverse resistivity anomalies in SrRuO₃

Daisuke Kan,[1,*] Takahiro Moriyama,[1,†] Kento Kobayashi,[1] and Yuichi Shimakawa[1,2]

[1]*Institute for Chemical Research, Kyoto University, Uji, Kyoto 611-0011, Japan*
[2]*Integrated Research Consortium on Chemical Sciences, Uji, Kyoto 611-0011, Japan*

We clarify the physical origin of anomalies in transverse resistivity often observed in exotic materials, such as SrRuO₃, in which the Berry curvature is manifested in the transport properties. The previously attributed mechanism for the anomalies, the topological Hall effect (THE) [e.g., J. Matsuno *et al.*, Sci. Adv. **2**, e160030 (2016)], is refuted by our thorough investigations as well as formulation of a model considering inhomogeneous magnetoelectric properties in the material. Our analyses fully explain every feature of the anomalies without resorting to the THE. The present results establish a fundamental understanding, which was previously overlooked, of magnetotransport properties in such exotic materials.

Materials and artificial heterostructures having a strong Dzyaloshinskii-Moriya (DM) interaction can host topologically nontrivial spin textures such as skyrmions [1,2]. Such topological magnetic textures can give rise to a Berry-curvature-originated fictitious magnetic field on electrons in motion and induce an additional transverse electron scattering known as the topological Hall effect (THE) [3–11]. While direct observation of nanometer-scale skyrmions is experimentally challenging [12–15], the existence of the skyrmions is often inferred from the THE observed with a simple transport measurement. In fact, recent reports [16–19] have discussed that the anomalies in the transverse resistivity of various materials and heterostructures, including multilayers of SrRuO₃ (SRO), are attributed to the THE due to the formation of skyrmions.

The perovskite SRO has intriguing electric properties originating from the strong spin-orbit interaction [20] together with the multiple band crossings around the Fermi level. Due to the temperature-dependent band crossings and their Berry curvatures, the temperature dependence of the anomalous Hall resistivity ρ_{AHE} does not simply follow that of the magnetization [21]. Most interestingly, ρ_{AHE} can become zero at a certain temperature (which we call T_S) while the magnetization is nonzero. SRO is therefore one of the rare materials in which one can identify an intrinsic anomalous Hall effect (AHE) originating from the Berry curvature [22].

In this study, we explore the transverse resistivity of single-layer films of SRO with different thicknesses (t_{SRO}) and epitaxially grown on NdGaO₃ (NGO) substrates. We particularly focus on SRO thickness t_{SRO} = 3–4.5 nm, the range in which the variation of T_S is significant. Every sample exhibits atypical humps, in the vicinity of T_S, in the transverse resistivity as a function of the applied magnetic field, which resemble what is called the THE [16–19,23,24]. However, based on our thorough investigations including the thickness dependence of the appearance of the humps, minor loop measurements of the transverse resistivity, and a numerical modeling, we discuss an alternative and more plausible mechanism explaining these anomalies.

We epitaxially grew SRO thin films on (110) NGO substrates by pulsed laser deposition. The SRO layer was deposited by pulsing SrRu$_{1.3}$O$_x$ targets with a KrF excimer laser (λ = 248 nm). We confirmed by x-ray diffraction measurements that the (110)-oriented SRO layer was coherently grown on the substrates (∼1.7% compressive strain). Very smooth step-and-terrace surface structures with single pseudocubic unit cell height steps (∼4 Å) were observed by atomic force microscopy. Longitudinal and transverse electrical resistivities (ρ_{xx} and ρ_{xy}) were measured by a conventional van der Pauw method.

Figure 1 shows temperature dependence of ρ_{xx} for t_{SRO} = 3–4.5 nm. For all the samples, ρ_{xx} overall decreases with decreasing temperature, indicating a metallic conduction. The ferromagnetic transition can be identified by the slight change in each curve in Fig. 1. We define the transition temperature T_C as the temperature at which the AHE vanishes (see Fig. 2, for example). It is found that T_C slightly decreases with decreasing t_{SRO}.

In contrast to the thickness dependence of ρ_{xx}, a slight difference in t_{SRO} significantly impacts on the behavior of ρ_{xy}. Figure 2 shows magnetic field H dependence of ρ_{xy} for t_{SRO} = 3.5 and 4.5 nm (the data set for t_{SRO} = 3 and 4 nm is provided in the Supplemental Material (SM) [25]). Note that the component of the ordinary Hall effect was subtracted from all the data shown in Fig. 2. The square hysteresis loop of the ρ_{xy}-H plots reflects the AHE in response to the magnetization switching. It is clear that there are two intriguing features in the hysteresis loops. One is that the squareness of the hysteresis loop as well as the polarity of ρ_{xy} varies with temperature. The other is that some atypical humps around the magnetization switching field are observed in a certain temperature range. Here we define the anomalous Hall resistivity ρ_{AHE} as the saturation resistivity in the positive field and also define ρ_{hump} as the height of the hump with
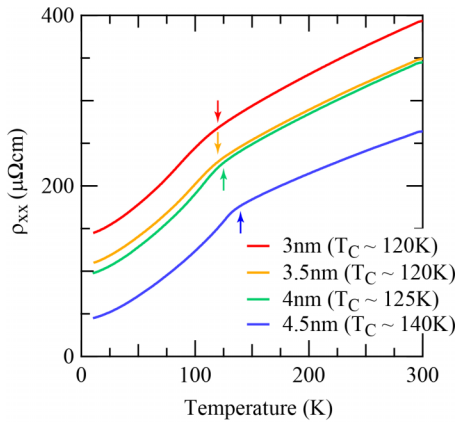
―――――――
*dkan@scl.kyoto-u.ac.jp
†mtaka@scl.kyoto-u.ac.jp

FIG. 1. Temperature dependence of ρ_{xx} for SRO films 3, 3.5, 4, and 4.5 nm thick.

respect to the saturation resistivity, and H_{ρ_peak} as the field at which the hump is positioned. These definitions are indicated in Fig. 2 (ρ_{AHE} can be either positive or negative, depending on the polarity of the hysteresis loop).

The sample with $t_{SRO} = 3.5$ nm ($T_C \sim 120$ K), for instance, shows a positive ρ_{AHE} at high temperature and undergoes reversal of the sign of ρ_{AHE} at $T_S = 68$ K, where T_S is defined as the temperature at which the sign of ρ_{AHE} reverses. Films with other thicknesses essentially show similar trends with different T_S values. The temperature dependence of ρ_{AHE} is consistent with the previous reports and originates from the temperature-induced changes in the integrated Berry curvature over the electron distributions around the Fermi level [21,22]. The humps seen in ρ_{xy}-H curves look quite similar to what were observed in previous reports [16,19,23,24] and were claimed to be due to the emergence of the THE. It should be emphasized that anomalies, essentially the same as
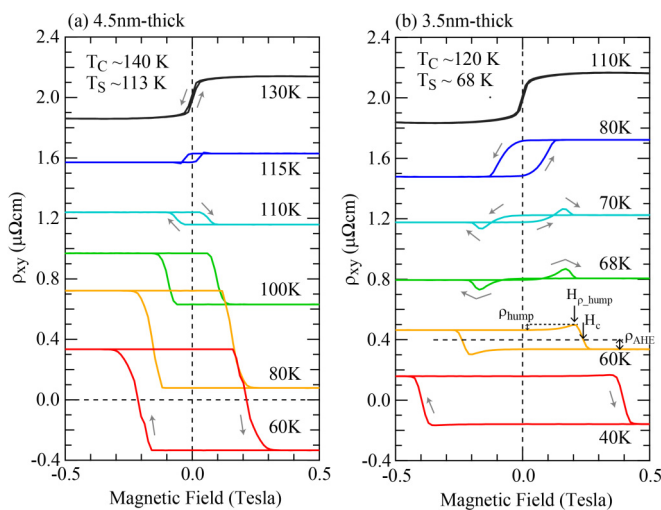

FIG. 2. Magnetic field dependence of ρ_{xy} for (a) 4.5- and (b) 3.5-nm-thick SRO films, exhibiting atypical humps around the magnetization switching field. The ρ_{xy}-H loops in the figures were obtained at various temperatures below the ferromagnetic transition temperature T_C (140 K for a 4.5-nm-thick film and 120 K for a 3.5-nm-thick film). Every loop in the figure has an offset of 0.4 $\mu\Omega$ cm.
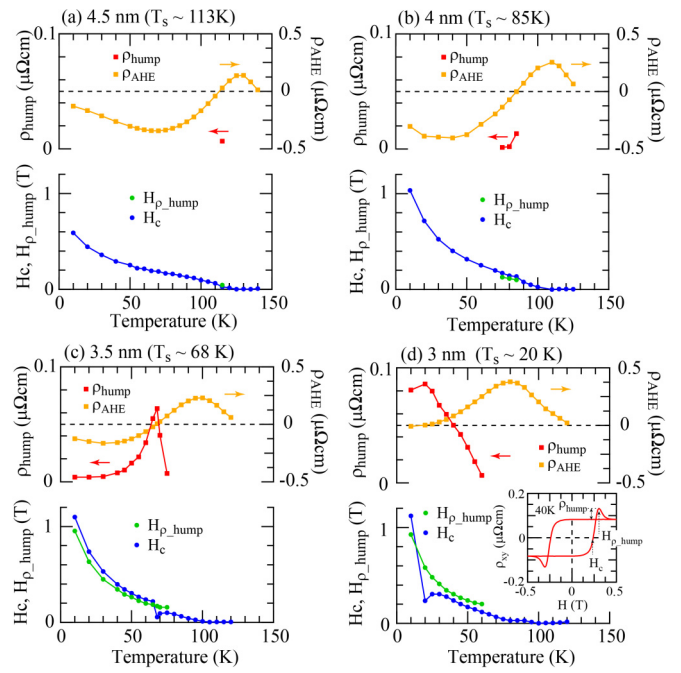

FIG. 3. ρ_{AHE}, ρ_{hump}, H_{ρ_hump}, and H_c as a function of temperature for SRO films (a) 3, (b) 3.5, (c) 4, and (d) 4.5 nm thick.

our observed humps, have been reported in SrIrO$_3$/SRO heterostructures [16,19], which are considered to host skyrmions due to a strong interfacial DM interaction. One may conceive that a structural asymmetry owing to the Ru-O-Ru bond angle variations [26,27] in the present sample can give rise to the DM interaction and form skyrmions, and therefore the THE could be present. In the following, however, we refute the THE mechanism and discuss an alternative physical origin for the appearance of the humps.

Figure 3 summarizes the temperature dependence of ρ_{hump}, H_{ρ_hump}, ρ_{AHE}, and H_c for $t_{SRO} = 3$–4.5 nm. ρ_{hump} is found to be always positive regardless of the film thickness. The maximum value of the ρ_{hump} increases with decreasing t_{SRO} and the temperature range where ρ_{hump} is seen also becomes wider as t_{SRO} decreases. It is found that ρ_{hump} is maximized at T_S, and concomitantly the H_c exhibits a discontinuity while H_{ρ_hump} smoothly changes across T_S. These behaviors of ρ_{hump} and H_c become more prominent for thinner films. We note that similar temperature dependences of ρ_{hump} are seen for the tensilely strained SrRuO$_3$ films on GdScO$_3$ (GSO) substrates [28]. Given that the types of the substrate-induced strain (either compressive or tensile) and spatial dependence of the Ru-O-Ru bond angle across the interface differ between the films on NGO and GSO, structurally induced properties of general interest, such as DM interaction, would be irrelevant to the emergence of the humps seen in ρ_{xy}-H plots.

We also investigated minor loops of ρ_{xy}-H for $t_{SRO} = 3$ nm at 20, 35, and 50 K. The results are summarized in Fig. 4. At each temperature, the loop starts from the positive field toward the negative field around which the hump appears and is folded back to the initial positive field. The maximum negative field in the minor loop measurements is referred to as H_{n_max}. We essentially found that the humps are hysteretic, meaning that the appearance of them depends on how the minor loop is

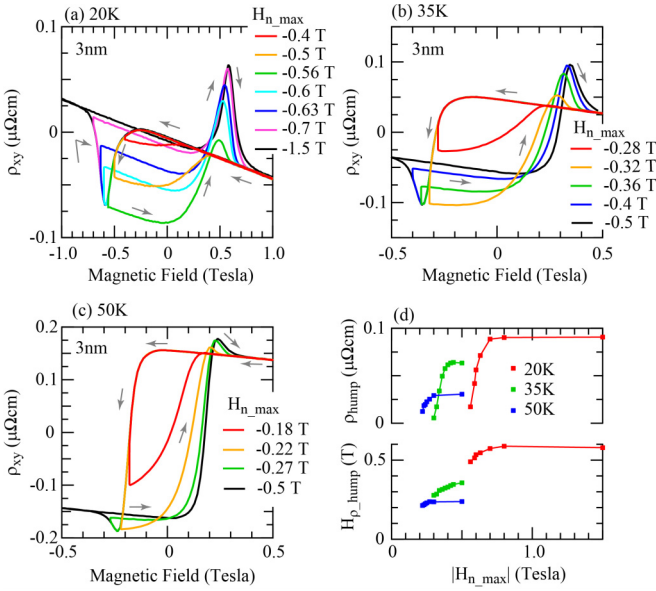FIG. 4. Minor loops of ρ_{xy} for the 3-nm-thick film, revealing the H_{n_max}-dependent appearance of the humps that cannot be in line with the story of the skyrmion formations leading to the THE. The loops were measured at (a) 20 K, (b) 35 K, and (c) 50 K. (d) ρ_{hump} and H_{ρ_hump} as a function of the maximum negative magnetic field H_{n_max}.

FIG. 5. (a) ρ_{AHE}-H hysteresis loops reproduced by our numerical model with $T_\sigma = 10.7$ K, highlighting that film inhomogeneities are the key for the atypical humps in ρ_{AHE}. For the calculations, ρ_{AHE} and H_c experimentally observed for the $t_{SRO} = 3.5$ nm film were used. (b) Temperature dependence of the calculated ρ_{hump}. (c) Reproduced minor loops at $T = T_S$.

scanned. For instance, looking at the loops at 20 K, where the humps are the most significant, one can see that the emergence of the humps in the positive field seems to depend on whether or not H_{n_max} surpasses magnetic fields in which the hump is seen. One clearly sees in the H_{n_max} dependence of the ρ_{hump} in the positive field shown in Fig. 4(d) that the ρ_{hump} decreases to zero when $|H_{n\_max}| < |H_{\rho\_hump}|$.

We point out that the H_{n_max}-dependent appearance of the humps cannot be in line with the story of the skyrmion formations leading to the THE unless one makes a rather convenient assumption that magnetic hysteresis in the skyrmions and the domains behaves as such [18]. Instead, we explain our overall experimental observations on the atypical humps by using a traditional magnetism taking into account the fact that ρ_{AHE} and H_c are strongly temperature dependent (see Fig. 3) and hypothesizing that they are inhomogeneous over the SRO film. We show in the following that those peculiar humps are indeed well reproduced by our model without considering the THE.

By starting with a simple toy model shown in the SM [25], the main features of the humps can already be reproduced by considering the two domains (domains A and B) that contain different T_S (T_{S_A} and T_{S_B}, respectively). Here we show a complete reproduction of the hysteresis loops by a more rigorous model taking into account multiple domains with a distribution of T_S denoted by T_σ.

Considering the temperature dependence of $\rho_{AHE}(T)$ and $H_c(T)$, one can write a field response of the transverse resistivity in each domain having a given effective temperature T' as

$$f(T', H) = \rho_{AHE}(T')\{1 - 2H_{Heav}[H - H_c(T')]\}g(T'),$$
(1)

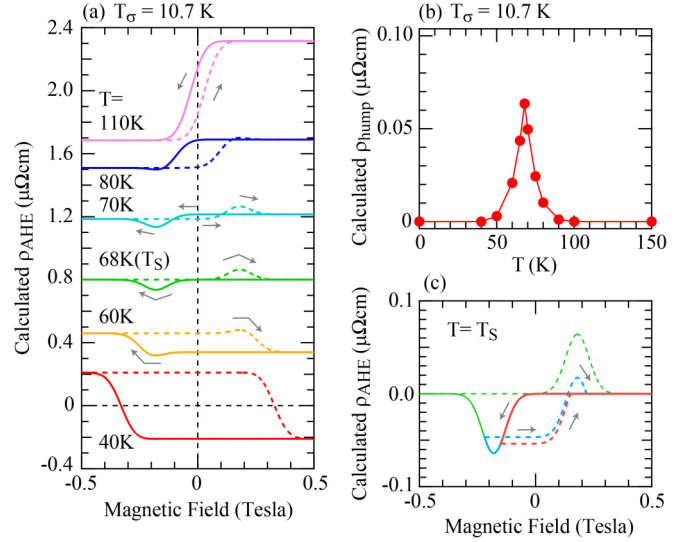where $H_{Heav}(x)$ is the Heaviside step function describing the magnetization switching and H is the applied field. $g(T')$ is the Gaussian function taking a distribution of the domain as

$$g(T') = \frac{1}{\sqrt{2\pi T_\sigma^2}}\exp\left[-\frac{(T' - T)^2}{2T_\sigma^2}\right].$$
(2)

Note that we implicitly assume that ρ_{AHE} and H_c are linear to T so that the actual spatial distribution of ρ_{AHE} and H_c can be mapped as a function of the effective temperature as $\rho_{AHE}(T')$ and $H_c(T')$ (see Fig. S3 in SM [25] for more detail). For our calculation, $\rho_{AHE}(T')$ and $H_c(T')$ are taken from the actual temperature dependence of ρ_{AHE} and H_c shown in Fig. 3 so that the only unknown parameter becomes T_σ.

The ρ_{AHE}-H plot at a measurement temperature T can be obtained by integrating $f(T', H)$ over T',

$$\Gamma(H) = \int_0^\infty f(T')dT'.$$
(3)

Note that, as $\Gamma(H)$ describes a magnetization switching in only one direction of the field sweep, the full loop is produced by taking another $\Gamma(H)$ for the other field sweep direction. Figure 5(a) shows the ρ_{AHE}-H loops calculated with $T_\sigma = 10.7$ K for the 3.5-nm-thick film. The hysteresis loops at various temperatures around T_S ($T_S = 68$ K for the 3.5-nm-thick film) reproduce very well our experimental observations [see Fig. 2(b)]. We also show in Fig. 5(b) that the temperature dependence of the ρ_{hump} extracted from the calculated loops [Fig. 5(a)] reproduces the experimentally obtained temperature dependence shown in Fig. 3. In particular, ρ_{hump} is found to be maximized at T_S and this behavior is exactly what is experimentally observed in the temperature dependence of the ρ_{hump}. Our model highlights that a spatial variation of T_S in the film essentially gives rise to a mixture of hysteresis loops with

both positive and negative ρ_{AHE} around T_S, consequently leading to the emergence of the humps which is totally irrelevant to THE or skyrmion formation.

Our model coherently explains the experimentally observed temperature-dependent ρ_{hump} for SRO films having other thicknesses (not shown). It is found that reducing t_{SRO} not only lowers T_S but also increases the inhomogeneity of T_S characterized by an increase of T_σ (see SM [25] for the estimation of T_σ). We also note that the minor loops of ρ_{xy}-H (Fig. 4) can also be reproduced well by our model. Representative loops are shown in Fig. 5(c), which clearly demonstrates that the humps in the positive field appear only when $|H_{n\_\mathrm{max}}|$ is greater than $|H_{\rho\_\mathrm{hump}}|$.

In summary, we showed that a single layer of SRO epitaxially grown on NGO substrates exhibits atypical humps in the transverse resistivity as a function of the external field, which resembles what has been claimed to be the topological Hall effect. However, our thorough investigations including the t_{SRO} dependence of the appearance of the humps, minor loop measurements, and numerical modeling indicate that the topological Hall effect cannot be the only origin of the observed humps. Our model, assuming a spatial variation of T_S in the film, reproduced every feature in the transverse resistivity very well, which strongly indicates that film inhomogeneities are the key factor responsible for the atypical humps. Our analysis further revealed that the variation of T_S as small as 10.7 K is enough to replicate the humps. We would like to emphasize that, based on our model, these atypical humps in the transverse resistivity could be observed in other materials, for example, rare earth–transition metal alloys [29,30], if T_S and H_{c} are spatially varied within a film. Finally, the present results provide a fundamental understanding of magnetotransport properties in such exotic materials, which would impact recently flourishing studies on topological materials.

[1] S. Mühlbauer, B. Binz, F. Jonietz, C. Pfleiderer, A. Rosch, A. Neubauer, R. Georgii, and P. Böni, Science **323**, 915 (2009).

[2] X. Z. Yu, Y. Onose, N. Kanazawa, J. H. Park, J. H. Han, Y. Matsui, N. Nagaosa, and Y. Tokura, Nature **465**, 901 (2010).

[3] M. Uchida and M. Kawasaki, J. Phys. D: Appl. Phys. **51**, 143001 (2018).

[4] S. Chakraverty, T. Matsuda, H. Wadati, J. Okamoto, Y. Yamasaki, H. Nakao, Y. Murakami, S. Ishiwata, M. Kawasaki, Y. Taguchi, Y. Tokura, and H. Y. Hwang, Phys. Rev. B **88**, 220405 (2013).

[5] A. Fert, N. Reyren, and V. Cros, Nat. Rev. Mater. **2**, 17031 (2017).

[6] C. Moreau Luchaire, C. Moutafis, N. Reyren, J. Sampaio, C. A. F. Vaz, N. Van Horne, K. Bouzehouane, K. Garcia, C. Deranlot, P. Warnicke, P. Wohlhüter, J. M. George, M. Weigand, J. Raabe, V. Cros, and A. Fert, Nat. Nanotechnol. **11**, 444 (2016).

[7] I. Kezsmarki, S. Bordacs, P. Milde, E. Neuber, L. M. Eng, J. S. White, H. M. Ronnow, C. D. Dewhurst, M. Mochizuki, K. Yanai, H. Nakamura, D. Ehlers, V. Tsurkan, and A. Loidl, Nat. Mater. **14**, 1116 (2015).

[8] Y. Ohuchi, Y. Kozuka, M. Uchida, K. Ueno, A. Tsukazaki, and M. Kawasaki, Phys. Rev. B **91**, 245115 (2015).

[9] N. Nagaosa and Y. Tokura, Nat. Nanotechnol. **8**, 899 (2013).

[10] M. Lee, W. Kang, Y. Onose, Y. Tokura, and N. P. Ong, Phys. Rev. Lett. **102**, 186601 (2009).

[11] A. Neubauer, C. Pfleiderer, B. Binz, A. Rosch, R. Ritz, P. G. Niklowitz, and P. Böni, Phys. Rev. Lett. **102**, 186602 (2009).

[12] A. Soumyanarayanan, M. Raju, A. L. Gonzalez Oyarce, A. K. C. Tan, M.-Y. Im, A. P. Petrovic, P. Ho, K. H. Khoo, M. Tran, C. K. Gan, F. Ernult, and C. Panagopoulos, Nat. Mater. **16**, 898 (2017).

[13] S. Woo, K. Litzius, B. Kruger, M.-Y. Im, L. Caretta, K. Richter, M. Mann, A. Krone, R. M. Reeve, M. Weigand, P. Agrawal, I. Lemesh, M.-A. Mawass, P. Fischer, M. Klaui, and G. S. D. Beach, Nat. Mater. **15**, 501 (2016).

[14] S. Woo, K. M. Song, X. Zhang, Y. Zhou, M. Ezawa, X. Liu, S. Finizio, J. Raabe, N. J. Lee, S.-I. Kim, S.-Y. Park, Y. Kim, J.-Y. Kim, D. Lee, O. Lee, J. W. Choi, B.-C. Min, H. C. Koo, and J. Chang, Nat. Commun. **9**, 959 (2018).

[15] W. Jiang, X. Zhang, G. Yu, W. Zhang, X. Wang, M. B. Jungfleisch, J. E. Pearson, X. Cheng, O. Heinonen, K. L. Wang, Y. Zhou, A. Hoffmann, and S. G. E. te Velthuis, Nat. Phys. **13**, 162 (2017).

[16] J. Matsuno, N. Ogawa, K. Yasuda, F. Kagawa, W. Koshibae, N. Nagaosa, Y. Tokura, and M. Kawasaki, Sci. Adv. **2**, e1600304 (2016).

[17] K. Yasuda, R. Wakatsuki, T. Morimoto, R. Yoshimi, A. Tsukazaki, K. S. Takahashi, M. Ezawa, M. Kawasaki, N. Nagaosa, and Y. Tokura, Nat. Phys. **12**, 555 (2016).

[18] B. M. Ludbrook, G. Dubuis, A. H. Puichaud, B. J. Ruck, and S. Granville, Sci. Rep. **7**, 13620 (2017).

[19] Y. Ohuchi, J. Matsuno, N. Ogawa, Y. Kozuka, M. Uchida, Y. Tokura, and M. Kawasaki, Nat. Commun. **9**, 213 (2018).

[20] G. Koster, L. Klein, W. Siemons, G. Rijnders, J. S. Dodge, C.-B. Eom, D. H. A. Blank, and M. R. Beasley, Rev. Mod. Phys. **84**, 253 (2012).

[21] Z. Fang, N. Nagaosa, K. S. Takahashi, A. Asamitsu, R. Mathieu, T. Ogasawara, H. Yamada, M. Kawasaki, Y. Tokura, and K. Terakura, Science **302**, 92 (2003).

[22] N. Nagaosa, J. Sinova, S. Onoda, A. H. MacDonald, and N. P. Ong, Rev. Mod. Phys. **82**, 1539 (2010).

[23] I. Lindfors-Vrejoiu and M. Ziese, Phys. Status Solidi B **254**, 1600556 (2017).

[24] B. Pang, L. Zhang, Y. B. Chen, J. Zhou, S. Yao, S. Zhang, and Y. Chen, ACS Appl. Mater. Interfaces **9**, 3201 (2017).

[25] See Supplemental Material at http://link.aps.org/supplemental/10.1103/PhysRevB.98.180408 for the ρ_{xy}-H plots for 4- and 3-nm-thick SRO films and details for our model to reproduce the experimentally observed ρ_{hump} behavior.

[26] R. Aso, D. Kan, Y. Shimakawa, and H. Kurata, Sci. Rep. **3**, 2214 (2013).

[27] R. Aso, D. Kan, Y. Fujiyoshi, Y. Shimakawa, and H. Kurata, Cryst. Growth Des. **14**, 6478 (2014).

[28] D. Kan and Y. Shimakawa, Phys. Status Solidi B **255**, 1800175 (2018).

[29] T. Okuno, K.-J. Kim, T. Tono, S. Kim, T. Moriyama, H. Yoshikawa, A. Tsukamoto, and T. Ono, Appl. Phys. Express **9**, 073001 (2016).

[30] J. Finley and L. Liu, Phys. Rev. Appl. **6**, 054001 (2016).